

Evolution of clustering structure through the momentum distributions in ^{8-10}Be isotopes

Songjie Li,^{1,*} Takayuki Myo,^{2,3,†} Qing Zhao,^{4,‡} Hiroshi Toki,³ Hisashi Horiuchi,³ Chang Xu,¹ Jian Liu,⁵ Mengjiao Lyu,^{3,§} and Zhongzhou Ren^{6,¶}

¹*School of Physics, Nanjing University, Nanjing 210093, China*

²*General Education, Faculty of Engineering, Osaka Institute of Technology, Osaka, Osaka 535-8585, Japan*

³*Research Center for Nuclear Physics (RCNP), Osaka University, Osaka 567-0047, Japan*

⁴*Department of Physics, Hokkaido University, Sapporo 060-0810, Japan*

⁵*College of Science, China University of Petroleum East China, Qingdao 266580, China*

⁶*School of Physics Science and Engineering, Tongji University, Shanghai 200092, China*

(Dated: May 12, 2020)

We investigate the evolution of clustering structure through the momentum distributions in the ^{8-10}Be isotopes. The nucleon dynamics within the inter-cluster antisymmetrization are discussed via the momentum distribution of a Brink type α - α wave function. For the state with a small α - α distance, we observe a significant depression with a dip structure at zero-momentum and an enhanced tail at relatively higher momentum region. In addition, we find the “cluster structure” in the intrinsic frame of momentum space, which is complementary to its significant α -cluster dissolution in the coordinate space because of the strong antisymmetrization. For the physical ^{8-10}Be isotopes, the Tohsaki-Horiuchi-Schuck-Röpke (THSR) wave functions are adopted. The evolution from the dilute clustering state to the compact one is demonstrated by a successive depression at the zero-momentum of nucleon distribution for the two α -clusters within ^{8-10}Be isotopes. For the compact ^{10}Be nucleus, the momentum distribution of all nucleons shows significant depression at zero-momentum with a dip structure, which is found to be contributed by both the inter-cluster antisymmetrization and the p -orbit occupation of the valence neutrons. This study proposes a new window for the investigations of the α -clustering effects via the low-momentum components of nuclei, which is expected to be extended to the heavier nuclear clustering states.

I. INTRODUCTION

In atomic nuclei, strongly correlated nucleons compose spatially localized subsystems, namely the nuclear clusters [1]. The relative motion between the α -clusters is the fundamental mode of dynamics in various nuclear systems, such as ^8Be , ^{12}C , ^{16}O , and ^{20}Ne . These clustering states have been studied by using different theoretical models, as reviewed in Refs. [2–11].

The Beryllium isotopes are well known for their clustering structures in the ground states, as discussed in previous theoretical studies [12–20]. In these works, many interesting physical phenomena, including the formation of two α clusters [13, 14], occupation of nuclear molecular orbits by the valence neutrons [12], di-cluster configurations [9], contribution from tensor force [16, 17], and non-localized dynamics of the two α -clusters [20], have been studied. It is found that the low lying spectrum of the ^{8-10}Be isotopes can be well described by the Tohsaki-Horiuchi-Schuck-Röpke (THSR) wave functions [18–20], which were originally proposed for the description of α -condensate states [26] and have been applied to many clustering phenomena in nuclei [18–25].

In previous works, the physical properties of cluster states in nuclei, such as the energy spectrum and the charge radii, have been reproduced by theoretical calculations. In addition, for probing the clustering effects, observables in various cluster-involved nuclear reactions have been investigated, such as the monopole transition strengths [27, 28], the proton induced α -knockout cross section [29, 30], and the α -emission cross sections in the fusion-evaporation reactions [31]. In this work, we propose to probe the evolution of the α -clustering structure through the momentum distributions in the ^{8-10}Be isotopes. In general, the momentum distributions could be extracted from the electron scattering reactions [32].

In recent decades, the electron scattering observables have been adopted to study the high-momentum components [32–35] or the deformation [36, 37] of nuclei. It is found that the tensor and short-range components of inter-nucleon correlations, induced by the nuclear force, dominate at the momentum regions at about 2 fm^{-1} and 4 fm^{-1} , respectively [38]. Comparing to the inter-nucleon correlations, the α -correlation dominates at much lower momentum region, and hence we may connect the α -cluster dynamics to the nucleon momentum distributions below the Fermi momentum of 1.4 fm^{-1} . Especially, due to the antisymmetrization effect between α -clusters, we expect that the momentum distribution would be depressed or enhanced in the compact systems where α -clusters have strong spatial overlap with each other, by analogy with the inter-nucleon contacts in the correlated NN pairs [39]. Through the momentum distributions

* songjie.li@smail.nju.edu.cn

† takayuki.myo@oit.ac.jp

‡ zhao@nucl.sci.hokudai.ac.jp

§ corresponding author: mengjiao@rcnp.osaka-u.ac.jp

¶ corresponding author: zren@tongji.edu.cn

in the ^{8-10}Be isotopes, we expect to reveal the evolution of the corresponding clustering structure, from the dilute gas-like state to the compact one with cluster dissolution.

For the theoretical description of Beryllium isotopes, we adopt the THSR wave function developed in our previous works [19, 20]. In Ref. [40], the momentum distribution of ^9Be was discussed through the Antisymmetrized Molecular Dynamics (AMD) wave function, but the center-of-mass component is not treated in the formulation. In this work, the momentum distributions are predicted by using the analytical derivation formulated recently in Ref. [38], with subtraction of center-of-mass motion.

This paper is organized as follows. In Sec. II, we introduce the formulation of the clustering wave functions and nucleon momentum distributions for the ^{8-10}Be isotopes. We note that the one-body momentum distributions of nucleons are investigated in this work, which are affected by the inter-nucleon and clustering correlations. In Sec. III A, the relation between the α - α distance and the nucleon momentum distribution is discussed through Brink type wave functions of two α -cluster system. In Sec. III B, we discuss the nucleon momentum distribution for the ^{8-10}Be isotopes predicted by using the physical THSR wave functions, and present their relation with the evolution of α -clustering structure. The last Sec. IV contains the conclusion.

II. FORMULATIONS

We introduce briefly the formulations for the clustering wave functions of the ^{8-10}Be isotopes and the corresponding nucleon momentum distributions. Detailed introductions can be found in Refs. [19, 20, 30] for the wave functions and in Ref. [38] for the nucleon momentum distributions.

A. Wave functions of ^{8-10}Be isotopes

We start by writing the Brink wave function of the ^8Be nucleus as [41]

$$\Psi^{\text{Brink}}(^8\text{Be}) = \sqrt{\frac{4! \cdot 4!}{8!}} \mathcal{A}\{\phi_{\alpha_1}(\mathbf{R}_1)\phi_{\alpha_2}(\mathbf{R}_2)\}, \quad (1)$$

where \mathcal{A} is the antisymmetrizer and the wave function of each alpha cluster $\phi_{\alpha}(\mathbf{R})$ is defined as

$$\phi_{\alpha}(\mathbf{R}) = \frac{1}{\sqrt{4!}} \mathcal{A}\{\phi_1(\mathbf{r}_1, \mathbf{R}) \dots \phi_4(\mathbf{r}_4, \mathbf{R})\}. \quad (2)$$

The single nucleon wave functions $\phi(\mathbf{r}, \mathbf{R})$ with the position \mathbf{r} are defined as the Gaussian wave packets

$$\phi(\mathbf{r}, \mathbf{R}) = (2\nu/\pi)^{3/4} e^{-\nu(\mathbf{r}-\mathbf{R})^2} \chi_{\sigma,\tau} \quad (3)$$

with centroids \mathbf{R} and width parameter $\nu = 0.27 \text{ fm}^{-2}$ to reproduce the binding energy of α -cluster. The component $\chi_{\sigma,\tau}$ is for the spin σ and isospin τ of each nucleon.

The Brink wave function in Eq. (1) describes the localized configuration of two α -clusters in the ^8Be nucleus. In physical nuclei, it is known that the α -clusters perform nonlocalized motion, which is confined by the Gaussian container in the THSR wave function [24]

$$\Psi^{\text{THSR}}(^8\text{Be}) = \int d\mathbf{R}_1 d\mathbf{R}_2 \mathcal{G}(\mathbf{R}_1, \beta_{\alpha}) \mathcal{G}(\mathbf{R}_2, \beta_{\alpha}) \times \mathcal{A}\{\phi_{\alpha,1}(\mathbf{R}_1)\phi_{\alpha,2}(\mathbf{R}_2)\}, \quad (4)$$

where the container function \mathcal{G} is the deformed Gaussian

$$\mathcal{G}(\mathbf{R}, \beta) = \exp\left(-\frac{R_x^2 + R_y^2}{\beta_{xy}^2} - \frac{R_z^2}{\beta_z^2}\right). \quad (5)$$

Here, the size of the Gaussian container is determined by the width parameters β_{xy} and β_z in each direction. For the $^{9,10}\text{Be}$ isotopes, we introduce additional valence neutrons into the THSR wave function as

$$\Psi^{\text{THSR}}(^9\text{Be}) = \int d\mathbf{R}_1 d\mathbf{R}_2 \mathcal{G}(\mathbf{R}_1, \beta_{\alpha}) \mathcal{G}(\mathbf{R}_2, \beta_{\alpha}) \times \mathcal{A}\{\phi_{\alpha,1}(\mathbf{R}_1)\phi_{\alpha,2}(\mathbf{R}_2)\phi_9^{\pi}\}, \quad (6)$$

$$\Psi^{\text{THSR}}(^{10}\text{Be}) = \int d\mathbf{R}_1 d\mathbf{R}_2 \mathcal{G}(\mathbf{R}_1, \beta_{\alpha}) \mathcal{G}(\mathbf{R}_2, \beta_{\alpha}) \times \mathcal{A}\{\phi_{\alpha,1}(\mathbf{R}_1)\phi_{\alpha,2}(\mathbf{R}_2)\phi_9^{\pi}\phi_{10}^{\pi}\}. \quad (7)$$

where $\phi_{9,10}^{\pi}$ are the wave functions of valence neutrons occupying π -orbits, which are formulated as

$$\phi_9^{\pi}(\mathbf{r}) = \int d\mathbf{R}_9 \mathcal{G}(\mathbf{R}_9, \beta_n) e^{i\phi_{\mathbf{R}_9}} \phi_{n\uparrow}(\mathbf{r}_9, \mathbf{R}_9), \quad (8)$$

$$\phi_{10}^{\pi}(\mathbf{r}) = \int d\mathbf{R}_{10} \mathcal{G}(\mathbf{R}_{10}, \beta_n) e^{-i\phi_{\mathbf{R}_{10}}} \phi_{n\downarrow}(\mathbf{r}_{10}, \mathbf{R}_{10}). \quad (9)$$

Here $\phi_{n\uparrow}$ and $\phi_{n\downarrow}$ are neutron wave functions defined in Eq. (3) with spin up and down, respectively, and $\phi_{\mathbf{R}}$ is the azimuthal angle of the neutron generator coordinate \mathbf{R} . The exponential factors $e^{\pm i\phi_{\mathbf{R}}}$ is introduced to reproduce the negative parity of the π -orbit [19]. More details for the formulation of Eqs. (8) and (9) can be found in Ref. [19]. The deformation parameters β are optimized by variational calculation for each isotope [19, 20].

B. Momentum distribution of the wave functions

The nucleon momentum distribution operator $\hat{n}(\mathbf{k})$ for mass number A is defined in the momentum space as

$$\hat{n}(\mathbf{k}) \equiv \sum_{i=1}^A \delta(\mathbf{k}_i - \mathbf{k}_G - \mathbf{k}), \quad (10)$$

where \mathbf{k}_i is the single-nucleon momentum and \mathbf{k}_G is the center-of-mass momentum

$$\mathbf{k}_G = \sum_{i=1}^A \mathbf{k}_i. \quad (11)$$

For the AMD wave functions [10]

$$\Psi^{\text{AMD}} = \mathcal{A} \left\{ \prod_{i=1}^A \phi_i(\mathbf{r}_i, \mathbf{R}_i) \right\}, \quad (12)$$

the nucleon momentum distribution with correct treatment for the center-of-mass motion is written as [38]

$$\begin{aligned} n(\mathbf{k}) &= \langle \Psi^{\text{AMD}} | \hat{n}(\mathbf{k}) | \Psi^{\text{AMD}} \rangle \\ &= \sum_{i=1}^A n_i(\mathbf{k}), \end{aligned} \quad (13)$$

where $n_i(\mathbf{k})$ is the momentum distribution of each nucleon

$$\begin{aligned} n_i(\mathbf{k}) &= \left(\frac{1}{2\pi\nu\epsilon} \right)^{3/2} \\ &\times \sum_{j=1}^A \exp \left[-\frac{1}{2\nu\epsilon} (\mathbf{k} - i\nu(\mathbf{R}_i^* - \mathbf{R}_j))^2 \right] B_{ij} B_{ji}^{-1}, \end{aligned} \quad (14)$$

$\epsilon = (A-1)/A$, and $B_{ij} = \langle \phi_i | \phi_j \rangle$ is the overlap matrix of single nucleon states. We note that in this formulation, the center-of-mass motion is correctly treated, as discussed in Ref. [38]. The momentum distribution $n(\mathbf{k})$ in Eq. (13) satisfies the normalization condition

$$\int d\mathbf{k} n(\mathbf{k}) = A. \quad (15)$$

Similarly, we define the proton momentum distribution as

$$n^P(\mathbf{k}) = \sum_{i \in p} n_i(\mathbf{k}), \quad (16)$$

where subscript i denotes all the protons. For the superposed AMD wave function $|\Psi\rangle = \sum_a c_a |\Psi_a\rangle$, the corresponding nucleon momentum distribution is given as

$$n(\mathbf{k}) = \frac{1}{\langle \Psi | \Psi \rangle} \sum_{a,b} c_a^* c_b \langle \Psi_a | \hat{n} | \Psi_b \rangle, \quad (17)$$

where c_a and c_b are superposition coefficients.

Mathematically, the Brink wave function in Eq. (1) can be written as a special case of the AMD wave function

$$\begin{aligned} \Psi^{\text{Brink}}(^8\text{Be}) &= \sqrt{\frac{1}{8!}} \mathcal{A} \{ \phi_1(\mathbf{r}_1, \mathbf{R}_1) \dots \phi_4(\mathbf{r}_4, \mathbf{R}_1) \\ &\quad \times \phi_5(\mathbf{r}_5, \mathbf{R}_2) \dots \phi_8(\mathbf{r}_8, \mathbf{R}_2) \}, \end{aligned} \quad (18)$$

which has the same format as Eq. (12). In addition, the THSR wave functions in Eqs. (4), (6), and (7) are mathematically equivalent to the superposed AMD wave

functions. As an example, we write the case for ^9Be as

$$\begin{aligned} \Psi^{\text{THSR}}(^9\text{Be}) &= \\ &\int d\mathbf{R}_1 d\mathbf{R}_2 \mathcal{G}(\mathbf{R}_1, \beta_\alpha) \mathcal{G}(\mathbf{R}_2, \beta_\alpha) \times \\ &\int d\mathbf{R}_9 \mathcal{G}(\mathbf{R}_9, \beta_n) e^{i\phi_{\mathbf{R}_9}} \times \\ &\mathcal{A} \{ \phi_1(\mathbf{r}_1, \mathbf{R}_1) \dots \phi_8(\mathbf{r}_8, \mathbf{R}_2) \phi_{n\uparrow}(\mathbf{r}_9, \mathbf{R}_9) \}. \end{aligned} \quad (19)$$

Hence, the momentum distributions of the Brink or THSR wave functions in this work can be calculated using the analytical formulations in Eqs. (13) and (17).

III. RESULTS

A. Nucleon momentum distribution of the α - α system

We first show the nucleon momentum distribution of two free α -clusters as the solid curve in Fig. 1. It is found that the momentum of free α -clusters distributes in a Gaussian form, which is the Fourier transformation of the α -cluster wave function in Eq. (2). We note that this Gaussian distribution is only valid in low momentum region less than the Fermi momentum $k_F = 1.4 \text{ fm}^{-1}$. As predicted in Ref. [38], the high-momentum region is dominated by the tensor and short-range correlations around $k \approx 2 \text{ fm}^{-1}$ and $k \approx 4 \text{ fm}^{-1}$, respectively. In this work, we focus on the clustering correlation and choose the effective Volkov NN interaction which does not include the tensor component or the short-range repulsion, and we limit our discussion on the momentum with up to k_F to avoid the effect from the high-momentum component. In addition, the G3RS term is adopted for the spin-orbit interaction. Parameters of the interactions are taken from Ref. [12].

For the ^8Be nucleus, we calculate the intrinsic momentum distribution along the z -axis described by the α - α Brink wave function in Eq. (1). This is a toy model with the relative motion of two α -clusters localized around the relative distance $\mathbf{D} = \mathbf{R}_1 - \mathbf{R}_2$. The z -axis is set as the symmetry axis, hence the relative distance of two α -clusters is determined by the parameter D_z . We show in Fig. 1 and 2 the nucleon momentum distributions of ^8Be with α - α distances $D_z = \{4, 3, 2, 1\} \text{ fm}$, which correspond to the evolution from the weak to the strong overlap between the two α -clusters.

In Fig. 1, the solid and dotted curves are used to illustrate the momentum distribution of two α -clusters without antisymmetrization between them, where the solid curve shows the distribution of two free α -clusters as discussed before, and the dotted one is for the α - α Brink wave function at infinite distance ($\mathbf{D} \rightarrow \infty$). These two curves have the Gaussian shape, but the one of the Brink wave function has an enhanced tail part and a smaller value at the zero momentum. This difference arises from the effect of the localization of the inter-cluster motion in

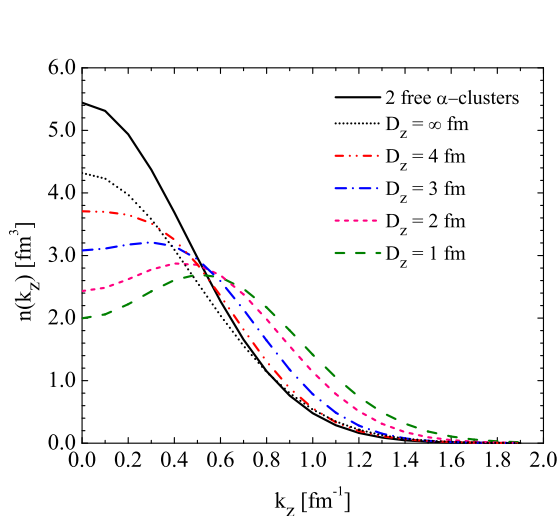


FIG. 1. The intrinsic momentum distributions of the ${}^8\text{Be}$ nucleus described by the Brink wave function along the z -axis. “ D_z ” is the relative distance between α clusters in z -axis. “2 free α -clusters” denotes the nucleon momentum distribution of two free α -clusters.

the α - α Brink wave function. Analytically using Eq. (14), we derive the momentum distribution $n(k)$ of two free α -clusters as

$$n_{2\alpha}^{\text{Free}}(\mathbf{k}) = \left(\frac{8}{3\pi\nu}\right)^{3/2} \exp\left(-\frac{2}{3\nu}\mathbf{k}^2\right), \quad (20)$$

where $\epsilon = 3/4$ for both α -clusters. For the α - α Brink wave function at infinite distance $D \rightarrow \infty$, we obtain

$$n_{2\alpha}^{\text{Infinite-Brink}}(\mathbf{k}) = \left(\frac{16}{7\pi\nu}\right)^{3/2} \exp\left(-\frac{4}{7\nu}\mathbf{k}^2\right), \quad (21)$$

where $\epsilon = 7/8$. The coefficient in Eq. (21) is smaller than the one in Eq. (20), which results in a smaller value at the center for the dotted curve as compared to the solid curve shown in Fig. 1.

For the curve with finite $D_z = 4$ fm in Fig. 1, a Gaussian shape, which is similar to the dotted curve with infinite D_z , is observed but with a slight depression near $k = 0$ fm $^{-1}$. This could be explained by the small overlap between two α -clusters and the nucleons are excited to the relatively higher momentum because of the inter-cluster antisymmetrization. By further reducing the α - α distance D_z , it is clearly seen that the momentum distribution becomes more peripheral and a dip structure appears at zero-momentum, which corresponds to a rather compact system where the nucleon excitation is most significant. This process, in which the Gaussian form of momentum distribution is broken, shows the dissolution of two α -clusters when they are in large spatial overlap with each other.

The nucleon dynamics within the overlapped α -clusters can be more clearly demonstrated by the intrinsic density distribution in the momentum space. The

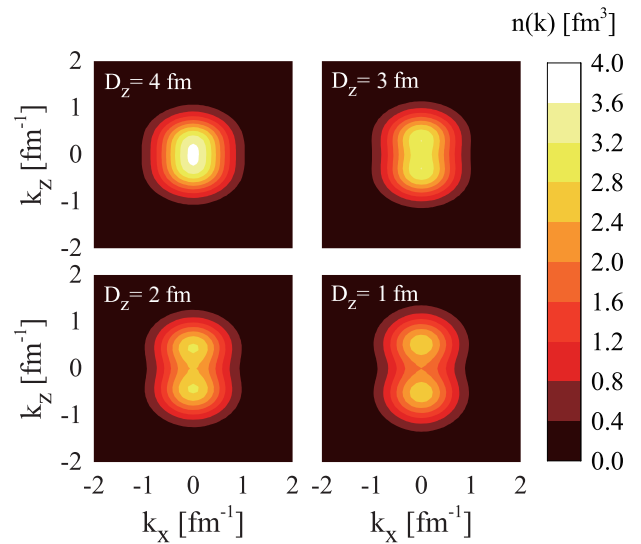


FIG. 2. The intrinsic nucleon momentum distributions of the α - α Brink wave function as functions of the α - α distance D_z in the x - z cross section.

corresponding density values in the x - z cross section are shown in Fig. 2 for different α - α distances D_z . With large distance $D_z = 4$ fm, the momentum distribution of two α -clusters is almost spherical, which is similar to the Gaussian distribution predicted for the free α -cluster. As the inter-cluster distance is decreased, the spherical symmetry is found to be broken and a large deformation of momentum distribution emerges. The most intriguing observation is that in the most compact configuration with $D_z = 1$ fm, a “cluster structure” is observed in the intrinsic momentum distribution of two α -clusters, which is astonishing when considering the fact that the α -clusters are strongly dissolved in the coordinate space under this short relative distance.

B. Nucleon momentum distribution of Beryllium isotopes

We calculate the nucleon momentum distribution for the 8 - ${}^{10}\text{Be}$ isotopes by using the corresponding THSR wave function for each nucleus, as formulated in Sec. II A. In our previous works [18–20], the accuracy of the THSR wave functions has been proved by reproducing the physical properties of the 8 - ${}^{10}\text{Be}$ isotopes, such as the energy spectra and radii. The Hamiltonian is adopted from Ref. [19] and the THSR wave function is variationally determined for each nucleus. The β parameters in the optimized THSR wave functions are listed in Table I. The resonant state of the ${}^8\text{Be}$ nucleus is simulated by a weakly bounded solution that corresponds to a local energy minimum in the variation of THSR wave function [18].

From Table I, it is clearly shown that the β parameter shrinks when introducing additional valence neutrons

TABLE I. Components of the deformation parameter β in the optimized THSR wave functions of ^{8-10}Be isotopes. All units are in fm.

	$\beta_{\alpha,xy}$	$\beta_{\alpha,z}$	$\beta_{n,xy}$	$\beta_{n,z}$
^8Be	1.0	11.0	-	-
^9Be	0.1	4.2	2.5	2.8
^{10}Be	0.1	2.5	1.9	2.9

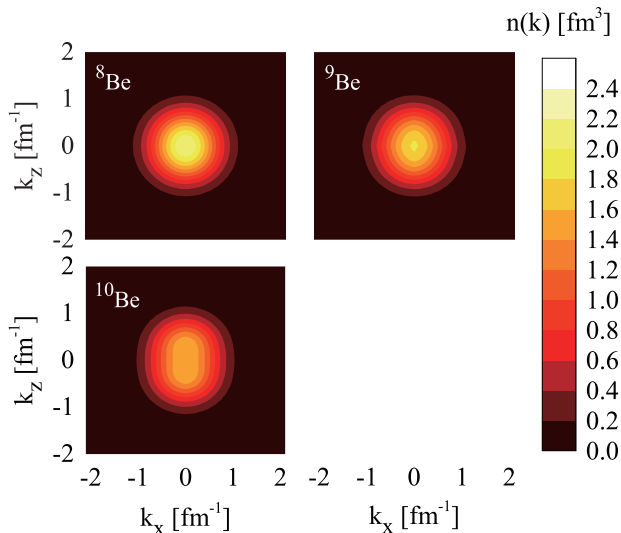


FIG. 3. The intrinsic proton momentum distributions of ^{8-10}Be isotopes in the x - z cross section.

into the nucleus, which corresponds to an evolution from the dilute cluster gas in ^8Be to the compact structure in ^{10}Be . The motion of α -clusters in the Be isotopes is demonstrated by the proton momentum distribution of ^{8-10}Be isotopes, as shown in Fig. 3. For the dilute ^8Be , we obtain spherical Gaussian distribution for the protons while clear deformation is observed for the compact ^{10}Be nucleus, which is similar to the Brink model discussed in Fig. 2. We note that the deformation in the THSR wave function of ^8Be is weaker than the Brink wave functions in Sec. III A, which is due to the spatially extended motion of α -clusters in ^8Be described by the THSR wave functions.

To obtain the distribution of two α -clusters for the ^{8-10}Be isotopes in the laboratory frame, we calculate the angle-averaged momentum distribution on the sphere surface S with the radius k , which is defined as

$$n(k) = \frac{1}{4\pi k^2} \int_{|\mathbf{k}|=k} n(\mathbf{k}) dS. \quad (22)$$

The THSR wave functions are adopted for the $^8\text{Be}(0_1^+)$, $^9\text{Be}(3/2_1^-)$, and $^{10}\text{Be}(0_1^+)$ isotopes after angular momentum projection [1], and the calculated distributions are shown in Fig. 4. In addition, corresponding curves for the intrinsic frames are also included for comparison, where

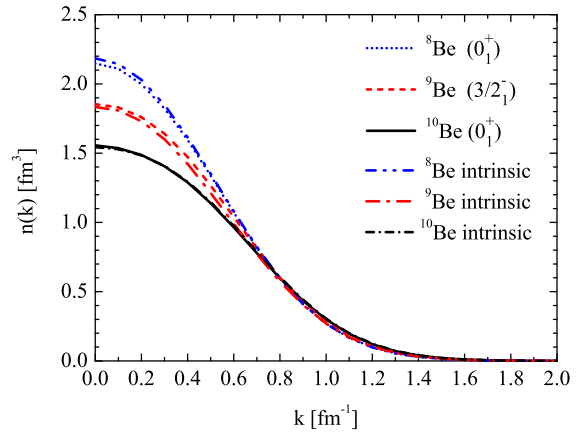


FIG. 4. The nucleon momentum distributions of the two α -clusters within the ^{8-10}Be isotopes. Curves denoted with parentheses are for the $^8\text{Be}(0_1^+)$, $^9\text{Be}(3/2_1^-)$, and $^{10}\text{Be}(0_1^+)$ nuclei in the laboratory frames. Curves denoted with “intrinsic” are for the intrinsic frames before angular momentum projections.

only slight differences before and after angular momentum projection are observed.

For the compact cluster state in ^{10}Be , the depression at zero-momentum and the enhanced tail region are observed once again in Fig. 4, as compared to the Gaussian-like curve of ^8Be . The depression in the distribution of the two α -clusters in ^{10}Be is not strong enough to produce a dip structure, but the large deviation from the ^8Be curve shows clearly the strong antisymmetrization between α -clusters. In ^9Be , relatively weaker α - α overlap is found from the intermediate zero-momentum depression.

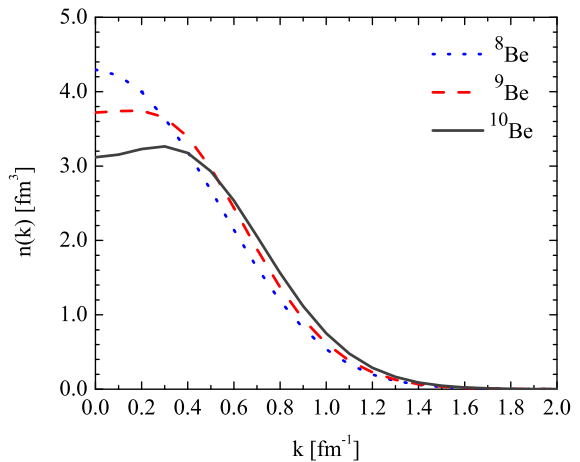


FIG. 5. The total momentum distributions of the $^8\text{Be}(0_1^+)$, $^9\text{Be}(3/2_1^-)$, and $^{10}\text{Be}(0_1^+)$ isotopes with THSR wave function.

We also calculate the momentum distribution of all nucleons in each isotope, as shown in Fig. 5. The solid curve for the ${}^8\text{Be}$ nucleus is not changed from Fig. 4, except the different amplitude. However, the dip structures appear in the curves of ${}^9\text{Be}$ and ${}^{10}\text{Be}$ isotopes, with further enhanced tail region, as compared to Fig. 4. In Ref. [32], similar dip structures have been observed in experimental results for ${}^{12}\text{C}$ and ${}^{16}\text{O}$ nuclei. We note that the dip structures in Fig. 5 are also contributed by the p -shell occupation by valence neutrons, in addition to the α - α antisymmetrization which is the major origin of dip structure in Fig. 1. This conjecture is proved by the decomposition of the momentum distribution in ${}^{10}\text{Be}$, as shown in Fig. 6. Here, the momentum component contributed by the α -clusters and the valence neutrons are calculated by replacing the summation over i in Eq. (13) with the corresponding set of nucleon indices. In this figure, the contribution from valence neutrons is presented by the blue dotted curve, in which the node structure of p -wave is clearly observed. It is also found that the valence neutrons contribute mostly around $k \approx 0.5 \text{ fm}^{-1}$, which enhances the tail region in Fig. 5. We note that using the relation $\langle k \rangle = 2\nu D$ in Ref. [42], this k corresponds to the high-momentum excitation of neutron with imaginary shift of about $D = 1 \text{ fm}$ in coordinate space, which is the mean location of valence neutron measured from the center of mass.

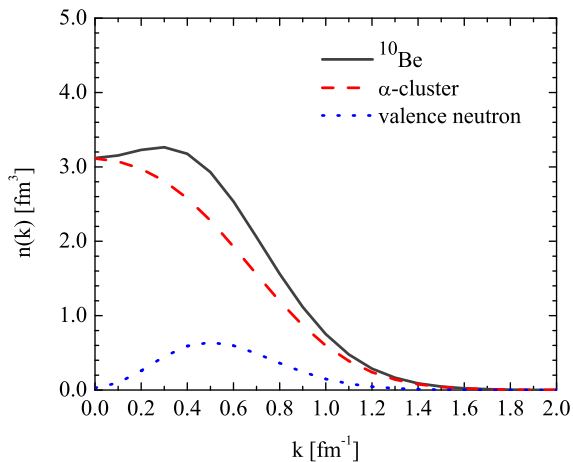


FIG. 6. Decomposition of momentum distributions in ${}^{10}\text{Be}$ (0_1^+) into components contributed by α -clusters and valence neutrons.

IV. CONCLUSION

We investigated the evolution of clustering structure through the momentum distributions in the ${}^{8-10}\text{Be}$ isotopes, which are calculated by using the analytical expressions formulated in our recent work. The general fea-

tures of the nucleon dynamics within two α -cluster system under antisymmetrization have been discussed via the momentum distribution of a Brink type α - α wave function. For the state with a strong inter-cluster overlap at small relative distance, we observed a significant depression with a dip structure at zero-momentum and an enhanced tail at relatively higher momentum region, which is a clear manifestation for the nucleon momentum excitation induced by the antisymmetrization between two α -clusters. The most interesting observation is that the momentum distribution of the extremely compact α - α system shows a “cluster structure” in the intrinsic frame of momentum space, which is complementary to its significant α -cluster dissolution in the coordinate space because of the strong antisymmetrization.

For the physical nuclei, we adopted the THSR wave functions for the clustering states in the ${}^{8-10}\text{Be}$ isotopes, which provided successful descriptions for these nuclei in our previous works. The evolution from the dilute gas-like state to the compact one with α -cluster dissolution was demonstrated by the calculated nucleon distribution for the two α -clusters within the Be isotopes, where the successive depression at zero-momentum was observed in the curves of ${}^9\text{Be}$, as compared to the curve of ${}^8\text{Be}$. We also calculated the momentum distribution of total nucleons for the ${}^{8-10}\text{Be}$ isotopes, and observe a significant depression at zero-momentum for the compact ${}^{10}\text{Be}$ nucleus. We performed the decomposition for the momentum distribution and found that both the inter-cluster antisymmetrization and the p -orbit occupation by the valence neutrons contribute to the dip structure at zero-momentum in the ${}^{10}\text{Be}$ nucleus. In this study, we propose a new window for the investigations of α -clustering structures in the ${}^{8-10}\text{Be}$ isotopes by connecting the lower region of momentum distributions with the nuclear clustering structures, which could be extended to the future studies of heavier nuclear clustering states.

ACKNOWLEDGMENTS

The authors would like to thank Prof. Hiroki Takemoto, Dr. Niu Wan, Prof. Masaaki Kimura and Prof. Bo Zhou for the valuable discussions, and also the anonymous reviewer for the valuable comments. This work is supported by the National Key Research and Development Program of China (Grants No. 2018YFA0404403 and No. 2016YFE0129300), the National Natural Science Foundation of China (Grants No. 11975167, No. 11961141003, No. 11761161001, No. 11535004, No. 11881240623, No. 11822503 and No. 11575082), the Science and Technology Development Fund of Macau under Grant No. 008/2017/AFJ, and the JSPS KAKENHI Grants No. JP18K03660. The author M.L. acknowledges the support from the RCNP theoretical group for his stay in RCNP and the fruitful discussions with the members, and the support from the Yozo Nogami Research Encouragement Funding. The author Q.Z. is grateful to

the members of the nuclear theory group in Hokkaido University for fruitful discussions.

-
- [1] H. Horiuchi and K. Ikeda, in *Cluster Models and Other Topics*, edited by T. T. S. Kuo and E. Osnes (World Scientific, Singapore, 1986), p. 1-258.
- [2] B. Zhou, Y. Funaki, H. Horiuchi, and A. Tohsaki, *Front. Phys.* **15**, 14401 (2019).
- [3] M. Freer, H. Horiuchi, Y. Kanada-En'yo, D. Lee, and Ulf-G. Meißner, *Rev. Mod. Phys.* **90**, 035004 (2018).
- [4] Z. Ren and B. Zhou, *Front. Phys.* **13**, 132110 (2018).
- [5] A. Tohsaki, H. Horiuchi, P. Schuck, and G. Röpke, *Rev. Mod. Phys.* **89**, 011002 (2017).
- [6] P. Schuck, Y. Funaki, H. Horiuchi, G. Röpke, A. Tohsaki, and T. Yamada, *Phys. Scr.* **91**, 123001 (2016).
- [7] M. Kimura, T. Suhara, Y. Kanada-En'yo, *Eur. Phys. J. A* **52** (2016) 373.
- [8] Y. Funaki, H. Horiuchi, and A. Tohsaki, *Prog. Part. Nucl. Phys.* **82**, 78 (2015).
- [9] M. Ito, and K. Ikeda, *Rep. Prog. Phys.* **77**, 096301 (2014).
- [10] Y. Kanada-En'yo, M. Kimura and A. Ono, *Prog. Theor. Exp. Phys.* **2012**, 01A202 (2012).
- [11] H. Horiuchi, K. Ikeda, and K. Kato, *Prog. Theor. Phys. Suppl.* **192**, 1 (2012).
- [12] N. Itagaki, S. Okabe, *Phys. Rev. C* **61**, 044306 (2000).
- [13] Y. Kanada-En'yo, H. Horiuchi, A. Ono, *Phys. Rev. C* **52**, 628 (1995).
- [14] Y. Kanada-En'yo, H. Horiuchi, A. Doté, *Phys. Rev. C* **60**, 064304 (1999).
- [15] M. Ito, K. Kato, K. Ikeda, *Phys. Lett. B* **588**, 43 (2004).
- [16] T. Myo, A. Umeya, K. Horii, H. Toki, and K. Ikeda, *Prog. Theor. Exp. Phys.* **2014**, 033D01 (2014).
- [17] T. Myo, A. Umeya, H. Toki, and K. Ikeda, *Prog. Theor. Exp. Phys.* **2015**, 63D03 (2015).
- [18] Y. Funaki, H. Horiuchi, A. Tohsaki, P. Schuck, and G. Röpke, *Prog. Theor. Phys.* **108**, 297 (2002).
- [19] M. Lyu, Z. Ren, B. Zhou, Y. Funaki, H. Horiuchi, G. Röpke, P. Schuck, A. Tohsaki, C. Xu, T. Yamada, *Phys. Rev. C* **91**, 014313 (2015).
- [20] M. Lyu, Z. Ren, B. Zhou, Y. Funaki, H. Horiuchi, G. Röpke, P. Schuck, A. Tohsaki, C. Xu, T. Yamada, *Phys. Rev. C* **93**, 054308 (2016).
- [21] Q. Zhao, Z. Ren, M. Lyu, H. Horiuchi, Y. Funaki, G. Röpke, P. Schuck, A. Tohsaki, C. Xu, T. Yamada, and B. Zhou, *Phys. Rev. C* **97**, 054323 (2018).
- [22] Q. Zhao, Z. Ren, M. Lyu, H. Horiuchi, Y. Kanada-Enyo, Y. Funaki, G. Röpke, P. Schuck, A. Tohsaki, C. Xu, T. Yamada, and B. Zhou, *Phys. Rev. C* **100**, 014306 (2019).
- [23] B. Zhou, Y. Funaki, H. Horiuchi, Z. Ren, G. Röpke, P. Schuck, A. Tohsaki, C. Xu, and T. Yamada, *Phys. Rev. Lett.* **110**, 262501 (2013).
- [24] B. Zhou, Y. Funaki, H. Horiuchi, Z. Ren, G. Röpke, P. Schuck, A. Tohsaki, C. Xu, and T. Yamada, *Phys. Rev. C* **89**, 034319 (2014).
- [25] B. Zhou, A. Tohsaki, H. Horiuchi, and Z. Ren, *Phys. Rev. C* **94**, 044319 (2016).
- [26] A. Tohsaki, H. Horiuchi, P. Schuck, and G. Röpke, *Phys. Rev. Lett.* **87**, 192501 (2001).
- [27] Z.H. Yang, Y.L. Ye, Z.H. Li et al., *Phys. Rev. Lett.* **112**, 162501 (2014).
- [28] Y. Chiba, M. Kimura, *Phys. Rev. C* **91**, 061302 (2015).
- [29] M. Lyu, K. Yoshida, Y. Kanada-En'yo, K. Ogata, *Phys. Rev. C* **97**, 044612 (2018).
- [30] M. Lyu, K. Yoshida, Y. Kanada-En'yo, K. Ogata, *Phys. Rev. C* **99**, 064610 (2019).
- [31] B. Wang, Z. Ren, and D. Bai, *Phys. Lett. B* **793**, 110 (2019).
- [32] C. Ciofi degli Atti and S. Simula, *Phys. Rev. C* **53**, 1689 (1996).
- [33] O. Hen et al, *Science* **346**, 614 (2014).
- [34] C. Ciofi degli Atti, *Phys. Rep.* **590**, 1 (2015).
- [35] O. Hen, G. A. Miller, E. Piasevsky, and L. B. Weinstein, *Rev. Mod. Phys.* **89**, 045002 (2017).
- [36] L. Wang, J. Liu, T. Liang, Z. Ren, C. Xu, and S. Wang, *J. of Phys. G* **47**, 025105 (2020).
- [37] J. Liu, R. Xu, J. Zhang, C. Xu, and Z. Ren, *J. of Phys. G* **46**, 055105 (2019).
- [38] M. Lyu, T. Myo, H. Toki, H. Horiuchi, C. Xu, and N. Wan, *Phys. Lett. B* **805**, 135421 (2020).
- [39] Q. Zhao, M. Lyu, Z. Ren, T. Myo, H. Toki, K. Ikeda, H. Horiuchi, M. Isaka, and T. Yamada, *Phys. Rev. C* **99**, 034311 (2019).
- [40] M. Hirai, S. Kumano, K. Saito, and T. Watanabe, *Phys. Rev. C* **83**, 035202 (2011).
- [41] D. M. Brink, in *International School of Physics "Enrico Fermi"*, XXXVI edited by C. Bloch (Academic Press, New York, 1966), p. 247.
- [42] T. Myo, H. Toki, K. Ikeda, H. Horiuchi, T. Suhara, M. Lyu, M. Isaka, T. Yamada, *Prog. Theor. Exp. Phys.* **2017**, 111D01 (2017).